Article

Thermal expansion and rattling behavior of Gd-filled Co_4Sb_{12} skutterudite determined by high-resolution synchrotron X-ray diffraction

J. E. Rodrigues [1,2,*], J. Gainza [2], F. Serrano-Sánchez [2], R. S. Silva Jr [3], C. Dejoie [1], N. M. Nemes [4], O. J. Dura [5], J. L. Martínez [2], J. A. Alonso [2,*]

1) European Synchrotron Radiation Facility (ESRF), 71 Avenue des Martyrs, 38000 Grenoble, France.
2) Instituto de Ciencia de Materiales de Madrid (ICMM), Consejo Superior de Investigaciones Científicas, Sor Juana Inés de la Cruz 3, E-28049 Madrid, Spain.
3) Department of Physics, Federal University of Sergipe, 49100-000, São Cristóvão-SE, Brazil.
4) Departamento de Física de Materiales, Universidad Complutense de Madrid, E-28040 Madrid, Spain.
5) Departamento de Física Aplicada, Universidad de Castilla-La Mancha, Ciudad Real, E-13071, Spain.

* Correspondence: rodrigues.joaoelias@gmail.com; rodrigues.joaoelias@esrf.fr; ja.alonso@icmm.csic.es.

Abstract: In this work, Gd-filled skutterudite $Gd_xCo_4Sb_{12}$ has been prepared in one-step method under high-pressure conditions in a piston-cylinder press at 3.5 GPa and moderate temperature of 800 °C. A detailed structural characterization was performed using synchrotron X-ray diffraction (SXRD), revealing a filling fraction of x = 0.066(4) and an average <Gd–Sb> bond length of 3.3499(3) Å. The lattice thermal expansion accessed via temperature-dependent SXRD led to a precise determination of a Debye temperature of 322(3) K, from the fitting of the unit-cell volume expansion using the second order Grüneisen approximation. Such parameter, when evaluated from the mean square displacements of Co and Sb, displayed a value of 265(2) K, meaning that the application of the harmonic Debye theory underestimates the Debye temperature in skutterudites. Regarding the Gd atom, its intrinsic disorder value is ~5× and ~25× higher than those of Co and Sb, respectively, denoting that Gd has a strong rattling behavior with an Einstein temperature of θ_E = 67(2) K. As a result, an ultra-low thermal conductivity of ~0.89 W/m·K at 773 K was obtained, leading to a thermoelectric efficiency zT of ~0.5 at 673 K.

Keywords: skutterudites; $CoSb_3$; thermal expansion; rattling effect; thermoelectrics.

1. Introduction

In recent times, an increasing energy demand has been observed as an unstoppable trend, making it necessary to seek for new energy sources or increasing the efficiency of the old ones. Approximately, about two thirds of the total energy production is wasted as heat, representing a frustratingly significant contribution that prevents achieving greater energy efficiency. Thermoelectric devices can transform useless heat into electrical energy directly and reversibly, and they could reduce the portion of wasted energy [1,2]. Thermoelectric generators have no moving parts, require minimum maintenance, and are much more reliable than most traditional power generation systems. However, before this technology becomes widespread, the conversion efficiency of the thermoelectric devices needs to be increased above the current ~5% [3–5]. This thermoelectric efficiency depends crucially on the material thermoelectric figure of merit, $zT = S^2\sigma T/\kappa$, where S stands for Seebeck coefficient, σ for electrical conductivity, κ for total thermal conductivity, and T for absolute temperature. Therefore, there is an intense search underway for novel materials with higher efficiency (zT) and other relevant properties (long term stability, thermal expansion, power-factor, price, environmental friendliness, etc.).

Thermoelectric materials are mainly sought among heavily doped semiconductors [6,7]. Among them, materials with skutterudite structure, derived from $CoSb_3$ pnictide, display a promising thermoelectric performance [8,9]. The binary skutterudite $CoSb_3$ (or Co_4Sb_{12}) is a narrow band-gap semiconductor thermoelectric (TE) material with excellent

 doi:10.20944/preprints202211.0389.v1

electrical performance. However, it shows high thermal conductivity due to the high covalency of the Co–Sb chemical bond, resulting in a very low zT value. Several strategies have been designed to reduce κ in skutterudites; the most extended is the so-called "filling" of the crystal structure [7,10–16].

The backbone of the skutterudite crystal structure is a framework of corner-sharing [$CoSb_6$] octahedra, heavily tilted in the three directions of the real space. This structure, defined in the $Im\bar{3}$ space group, contains large voids at 2*a* sites, where distinct elements like rare earth, alkali earth or alkali cations can be lodged, in overdimensioned cavities where the effect of "rattling" of these filler elements drastically reduces the lattice thermal conductivity in filled skutterudites [8]. According to the PGEC theory (phonon-glass, electron-crystal) materials [17,18], this "ball in a cage" configuration of filled skutterudites directly determines the basic conditions for high zT values.

In precedent works, we have successfully synthesized and characterized such compounds under high-pressure conditions, given the metastable character of these distorted compounds. For instance, Co_4Sb_{12} can be stabilized at 3.5 GPa, finding exceptionally low thermal conductivities that were ascribed to partial Sb deficiency, the Sb vacancies acting as phonon scatterers [19]. We also stabilized $La_xCo_4Sb_{12}$, La acting as rattler element [20]. Subsequently, other $M_xCo_4Sb_{12}$ pnictide skutterudites were filled with a panoply of rare-earths (Ce, Yb, Y, mischmetal), alkali earth (Sr) or alkali elements (K) which were successfully introduced in the 2*a* skutterudite cages, at hydrostatic pressures of 3.5 GPa at moderate temperatures [21–25].

Previous works have devoted their attention for Gd-filled skutterudites, $Gd_xCo_4Sb_{12}$, particularly: Yang *et al.* described the thermoelectric performance of high-pressure obtained $Gd_{0.12}Co_4Sb_{12}$ with a highest zT = 0.52 at 600 K [26]; Liu *et al.* investigated the thermoelectric properties of $Gd_xFe_yCo_{4-y}Sb_{12}$ skutterudites prepared by melting-annealing method, showing empirically the role of Gd to dramatically reduce the thermal conductivity [27]. However, a more careful structural determination was needed to probe the temperature-dependent lattice dynamics in Gd-filled skutterudites and the rattling effect of Gd atom. Here, we describe a Gd-filled skutterudite, $Gd_xCo_4Sb_{12}$, prepared at 3.5 GPa, where high-angular resolution synchrotron X-ray diffraction (SXRD) data disclosed conspicuous features that account for a substantial reduction of the thermal conductivity in this thermoelectric material.

2. Experimental Methods

A nominal composition of $Gd_{0.5}Co_4Sb_{12}$ was synthesized by a solid-state reaction under high-pressure and moderate temperature conditions. About 1.2 g of a stoichiometric mixture of the starting elements Gd (99.0%, Alfa Aesar), Co (99 %, ROC/RIC), and Sb (99.5 %, Alfa Aesar) were ground and placed in a niobium capsule (of 5 mm in diameter), sealed, and inserted inside a cylindrical graphite heater. The capsule was manipulated inside an Argon-filled glove box. Reactions were carried out in a piston-cylinder press (Rockland Research Co.), at a pressure of 3.5 GPa, at 800 °C for 1 h. Afterwards, the products were quenched to room temperature and the pressure was released. The recovered sample was obtained as hard pieces, which were partially ground into fine powder for structural characterization or cut with a diamond saw to perform transport measurements.

High-resolution synchrotron X-ray diffraction (SXRD) patterns were recorded at the beamline ID22 at the European Synchrotron Radiation Facility (ESRF, Grenoble). The incident X-ray radiation wavelength was set to 0.35418 Å. The temperature interval between 10 and 1000 K was covered using a He-cooled cryostat and a hot-air blower, with the powder sample loaded into quartz capillaries of 0.5 mm in diameter. The diffraction patterns were collected over the 2θ 1°–40° range with a multi-analyzer stage of 13 Si(111) crystals. High-resolution powder diffraction patterns were retrieved following the procedure described in Ref. [28]. Rietveld refinements were carried out using the *FullProf* pro-

Preprints (www.preprints.org) | NOT PEER-REVIEWED | Posted: 21 November 2022 doi:10.20944/preprints202211.0389.v1

gram and the peak shape was described using a pseudo-Voigt function [29]. The refinement included the following parameters: scale factors, zero-point error, background coefficients, asymmetry correction factors, lattice parameters, atomic positions, occupancy factors, and isotropic displacement parameters.

The Seebeck coefficient was determined using a commercial MMR-technologies system. Measurements were recorded under vacuum from room temperature up to 800 K. A constantan wire was used as a reference for comparison with bar-shaped skutterudite samples cut with a diamond saw perpendicular to the pressing direction. The reproducibility was verified with different contacts and constantan wires. A Linseis LFA 1000 instrument was used to measure the thermal diffusivity (α) of the samples over a temperature interval $300 \leq T \leq 800$ K by the laser-flash technique. A thin graphite coating was applied to the surface of the pellet to maximize heat absorption and emissivity. The thermal conductivity (κ) is determined using $\kappa = \alpha \cdot C_P \cdot \rho_p$, where C_P is the specific heat and ρ_p is the sample physical density. Then, the specific heat was calculated using the Dulong-Petit equation.

3. Results and Discussion

3.1. Crystal structure

The crystal structure of the as-obtained Gd-filled Co_4Sb_{12} was probed from high-resolution SXRD data. The unit-cell was indexed at room temperature by following the symmetry restriction of the body-centered space group $Im\bar{3}$ (#204, T_h^5) with lattice parameter a = 9.042849(7) Å, as shown in **Fig. 1a**. With eight formula per unit-cell (Z = 8), the atoms are distributed as follows: Co at 8*c* ($\bar{3}$) sites [0.25, 0.25, 0.25], Sb at 24*g* (m) sites [0, y = 0.33511(3), z = 0.15792(3)], and Gd at 2*a* ($m\bar{3}$) sites [0, 0, 0]. The crystal structure of the Gd-filled Co_4Sb_{12} is shown in **Fig. 1c** and **Fig. 1d**, which highlight the distorted octahedral units [$CoSb_6$] and the Sb rings [Sb_4] formed as a consequence of the strong tilting of the octahedra, respectively. It was determined that the nominal composition x = 0.5 was not reached, instead a filling fraction of x = 0.066(4) was obtained, leading to the chemical formula $Gd_{0.066(4)}Co_4Sb_{12}$. No secondary (or minor) phases were detected. **Table 1** summarizes the refined parameters at room temperature, besides the bond lengths Co–Sb, Gd–Sb, and Sb–Sb. The last one has two values for describing the rectangular shape of the ring [Sb_4].

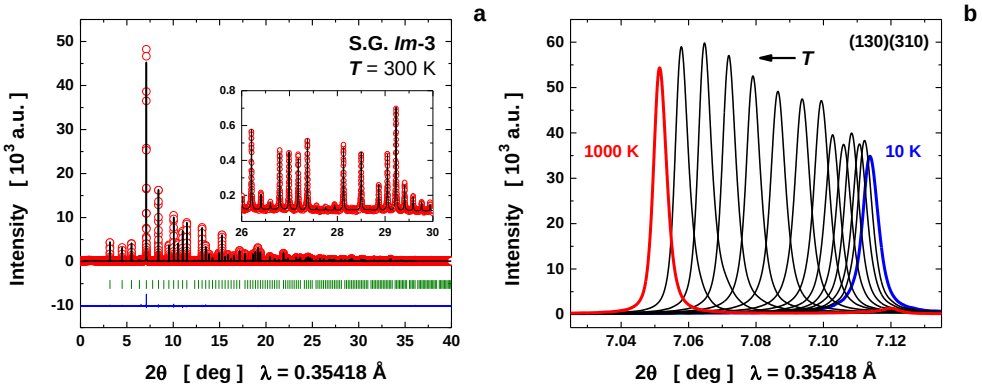

Preprints (www.preprints.org) | NOT PEER-REVIEWED | Posted: 21 November 2022 doi:10.20944/preprints202211.0389.v1

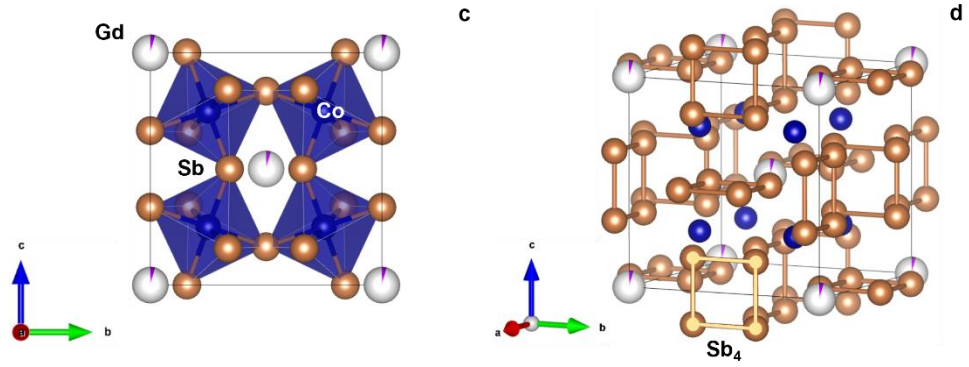

Figure 1. (a) Rietveld refinement of the synchrotron X-ray diffraction pattern of Gd-filled Co_4Sb_{12} skutterudite at room temperature. **(b)** Temperature evolution in the range 10–1000 K of the main reflection (130)(310). In part **(a)**, red open circles are the experimental data, black line denotes the calculated profile, blue line is the difference between experimental and calculated data, and dark green bars the Bragg reflections. Crystal structure representation exhibiting **(c)** the octahedral units [$CoSb_6$] and **(d)** the Sb rings [Sb_4].

Then, a precise temperature-dependent evaluation was carried out in the Gd-filled Co_4Sb_{12} skutterudite to probe its thermal expansion and thermoelastic properties from 10 up to 1000 K. As expected, no phase transition was observed and only the volume expansion could be detected as exemplified in **Fig. 1b** through shifts to lower angles of the main reflection (130)(310).

Table 1. Refined structural parameters of the Gd-filled Co_4Sb_{12} skutterudite from SXRD data at room temperature. *Abbreviations*: U_{eq} is the equivalent mean square displacement, SOF the site occupancy factor, and ρ_t the theoretical density.

Atom	Wyckoff	x	y	z	U_{eq} (10^{-3} Å^2)	SOF
Co	8*c*	0.25	0.25	0.25	7.4(1)	1
Sb	24*g*	0	0.33511(3)	0.15792(3)	7.05(4)	1
Gd	2*a*	0	0	0	28(7)	0.033(2)
Unit-cell parameters		*Bond lengths*			*Reliability factors*	
a (Å)	9.042849(7)	d_0 (Co–Sb) (Å)	2.5291(3)		R_p (%)	6.30
V (Å^3)	739.4619(10)	d_1 (Sb–Sb) (Å)	2.8561(4)		R_{exp} (%)	4.94
ρ_t (g.cm^{-3})	7.644(1)	d_2 (Sb–Sb) (Å)	2.9823(4)		R_{wp} (%)	6.86
		d_3 (Gd–Sb) (Å)	3.3499(3)		R_{Bragg} (%)	1.92

3.2. Thermoelastic properties

Considering the absence of any structural transition at low and high temperatures in $Gd_{0.066(4)}Co_4Sb_{12}$, we can proceed to evaluate both thermal expansion and thermoelastic properties of this compound. The available data cover the temperature range of 10–1000 K, which enables a second order expansion of the Grüneisen approximation. In this method, the anharmonic contributions from the lattice vibration are considered and the thermal expansion of unit-cell volume $V(T)$ has similar description to the elastic strain and can be second order expanded, as follows [30]:

$$V(T) = V_0 + \frac{V_0\, U(T)}{Q - b\, U(T)} \quad (1)$$

such that, V_0 denotes the unit-cell volume at 0 K, $Q = \frac{V_0 B_0}{\gamma'}$, $b = \frac{B_0' - 1}{2}$, B_0 and B_0' are the bulk modulus and its first derivative in pressure at 0 K, and γ' describes the Grüneisen parameter. γ' is zero for an harmonic crystal, and $\gamma' \neq 0$ when anharmonic effects occur typically at high-temperatures [31]. The function $U(T)$ represents the internal energy as derived from the Debye theory, i.e.

Preprints (www.preprints.org) | NOT PEER-REVIEWED | Posted: 21 November 2022 doi:10.20944/preprints202211.0389.v1

$$U(T) = 9N_a k_B T \left(\frac{T}{\theta_D}\right)^3 \int_0^{\theta_D/T} \frac{z^3}{e^z - 1} dz \quad (2)$$

where, N_a is the total number of atoms within the unit-cell (in the case of $CoSb_3$, N_a = 32), θ_D the Debye temperature, k_B and T maintain their usual meaning in physics.

Using the previous equations, we fitted the volume expansion with temperature in **Fig. 2a**, where the following parameters were obtained: θ_D = 322(3) K, V_0 = 735.310(3) Å^3, Q = 4.41×10^{-17} J, and b = 0.764. The comparison between the experimental and fitted curves shows a good agreement in the entire temperature interval. In this model, Q and b are assumed to be temperature-independent. By taking literature value for the bulk modulus (B_0) in $CoSb_3$ of 100(4) GPa [25], the Grüneisen parameter (γ') can be estimated around 1.67(5), which partially agree with the value 1.11(1) for $CoSb_3$ as extracted from the compressibility data at a constant temperature [32]. Still, a larger value indicates anharmonic bonding and stronger phonon-phonon interactions, which account for the reduced lattice thermal conductivity [33]. In addition, the first derivative B_0' is evaluated as 2.5(3). This result points out that the anharmonicity of the lattice vibrations at high-temperature may be an important parameter to describe the thermoelectric performance in filled skutterudites.

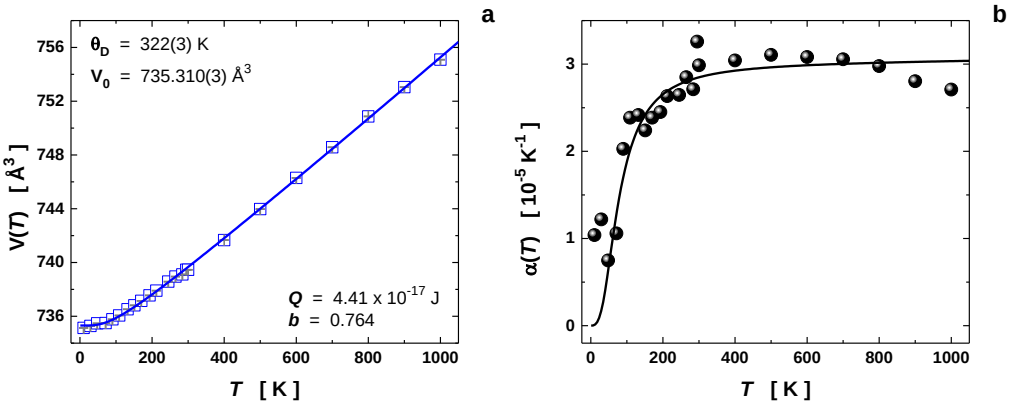

Figure 2. (a) Thermal expansion of the unit-cell volume $V(T)$, such that the solid line is the second order Grüneisen approximation to the zero-pressure equation of state. **(b)** Thermal expansion coefficient $\alpha(T)$, where the spheres were obtained by numerical first derivative of the unit-cell volume and the black solid line is the calculated from the fitted unit-cell volume expansion using Eq (1).

From the first derivative of the unit-cell volume, the thermal expansion coefficient $\alpha(T)$ can be evaluated [30], as follows:

$$\alpha(T) = \frac{1}{V}\frac{dV}{dT} \quad (3)$$

Fig. 2b compares the experimental values for $\alpha(T)$ (numerical first derivative of the experimental points) and the calculated thermal expansion coefficient from the fitting using Eq (1). One may see that, for temperatures above 800 K, the experimental points start to depart from the calculated thermal expansion coefficient, possibly caused by the internal instabilities of the filler element Gd, which can result in thermal decomposition for temperatures higher than 1000 K [19,22].

3.3. Mean square displacement

The Debye approximation can also be used to describe the thermal evolution of the principal thermal vibration parameters after converted to the mean square displacements (MSDs or U_{eq}, in units of Å^2) [34–36], as defined by:

Preprints (www.preprints.org) | NOT PEER-REVIEWED | Posted: 21 November 2022 doi:10.20944/preprints202211.0389.v1

$$U_{eq}(T) = d_s^2 + \frac{3\hbar^2 T}{mk_B\theta_D^2}\left[\frac{T}{\theta_D}\int_0^{\theta_D/T}\frac{z}{e^z-1}dz + \frac{\theta_D}{4T}\right] \quad (4)$$

where d_s^2 is the intrinsic disorder (also known as the static displacement at 0 K), m the atom's mass, and the $\hbar$ the reduced Planck constant. This Debye model evaluation is more appropriate for Co and Sb atoms because such atoms constitute the framework (or the lattice) of the skutterudite structure, see **Fig. 1c**.

Co atom exhibited an intrinsic disorder of 1.65(7)×10^{-3} Å^2 and a Debye temperature of θ_D = 393(1) K. On the other hand, Sb atom shows an intrinsic disorder of 5.72(8) ×10^{-4} Å^2 and a Debye temperature of θ_D = 240(1) K. These values for θ_D, after averaged by the atomic masses of Co and Sb, provide a Debye temperature for the framework of θ_D = 265(2) K, which agrees with previous values for $CoSb_{3-\delta}$ (θ_D = 262 K) [19] and other partially filled skutterudites (θ_D = 265–274 K) [37], which were also extracted from MSDs analyses. Our result of θ_D = 265(2) K is in partial agreement with the Debye temperatures obtained from the heat capacity curves (θ_D = 280–294 K) [37]. However, the Debye temperature evaluated from both volume expansion and MSDs displayed quite different values, i.e. 322(3) and 265(2) K, respectively. This difference originates at the evaluation method of the Debye temperature, being this discrepancy also noticed by Vočadlo *et al.* for ε-FeSi [30]. As a result, the thermal expansion fitting of the unit-cell volume is indeed very sensitive to the temperature range and anharmonic effects [30], which may explain such differences. It denotes that the application of only harmonic Debye approximation may underestimate the Debye temperature in skutterudites.

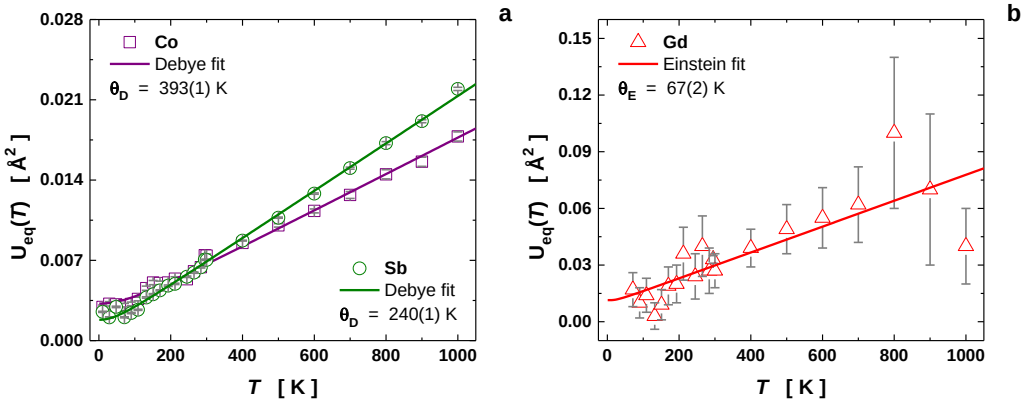

Figure 3. Temperature-dependence of the mean square displacements $U_{eq}(T)$ (or MSDs in units of Å^2) for the atoms **(a)** Co, Sb and **(b)** Gd. The Co–Sb framework was evaluated using the Debye approximation, while the dynamic behavior of the filler Gd was fitted to the Einstein model.

Gd atom has a less chemically bound situation at 2*a* sites (voids), enabling its rattling behavior [38], which works for the benefit of the acoustic phonon scattering, thus reducing the thermal conductivity [23,37,39]. In such a case, the normal vibrations can be treated as independent oscillators according to the Einstein approximation, as follows:

$$U_{eq}(T) = d_s^2 + \frac{\hbar^2}{2mk_B\theta_E}\coth\left(\frac{\theta_E}{2T}\right) \quad (5)$$

where θ_E denotes the Einstein temperature. The fitted value for the intrinsic disorder d_s^2 approaches 9.1(2)×10^{-3} Å^2, which is about ~5× and ~25× higher than those values for Co and Sb, respectively. This result shows that Gd has a strong rattling effect at the 2*a* voids, being corroborated by the Einstein temperature θ_E = 67(2) K. This low value agrees with those for typical fillers of rare-earth elements, normally ranging from 54–88 K [20,22,37]. Specially, the θ_E value for Gd is close to that for Eu, i.e. θ_E = 68(2) K [37], both elements having similar atomic masses. In **Fig. 3b**, a slope change in the Gd MSD is seen at 800 K,

Preprints (www.preprints.org) | NOT PEER-REVIEWED | Posted: 21 November 2022 doi:10.20944/preprints202211.0389.v1

which may be associated with internal instabilities of the filler in view of the high U_{eq} value of 0.1(6) Å^2.

3.4. Local atomic bonding

As established in the literature [24,40,41], the skutterudite-type structure belonging to the space-group $Im\bar{3}$ is fully described by three parameters, namely the lattice constant a and the Sb fractional coordinates y and z. While the lattice constant is sensitive to the filling fraction, the Sb fractional coordinates can be used to probe the topology of the [Sb$_4$] ring [23]. For a square ring, where the short (d_1) and long (d_2) Sb–Sb distances have the same length, the coordinates are constrained to $z + y = 0.5$ (Oftedal line) [42]. **Fig. 4a** displays the Oftedal plot (z *vs.* y) for both Gd-filled and unfilled Co$_4$Sb$_{12}$ (from ref. [19]). One may see two tendencies: 1) the incorporation of the filler brings the Sb ring closer to the Oftedal line, 2) the temperature increase induces a ring deformation from a square to a more rectangular shape. This behavior was also observed by Hanus *et al*. for Yb-filled Co$_4$Sb$_{12}$ [41].

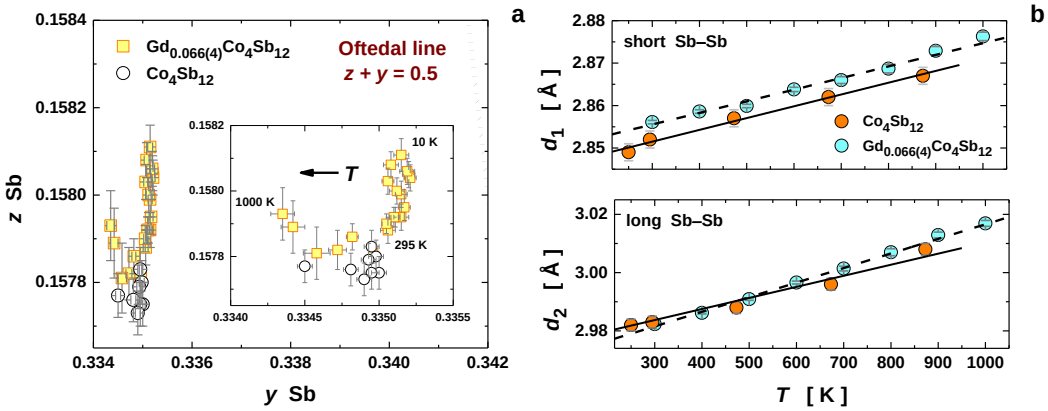

Figure 4. (a) Oftedal plot with the Oftedal line (red dotted line, such that $z + y = 0.5$) comparing both Gd-filled and unfilled Co$_4$Sb$_{12}$. **(b)** Temperature dependence of the short and long Sb–Sb distances in the [Sb$_4$] ring for both Gd-filled and unfilled Co$_4$Sb$_{12}$.

The different temperature evolution of the [Sb$_4$] ring bonds distances (**Fig. 4b**) are analyzed using the local linear expansion coefficients (**Table 2**), calculated as $\alpha_l(T) = \frac{1}{l}\frac{dl}{dT}$. These provide an indication of the electron density between the atoms and the respective bond strength, as weaker bonds will show a more pronounced expansion with temperature [41]. Here, a significant increase of the short Sb–Sb bond distance at room temperature is observed after filling; however, the local expansion coefficient remains analogous to unfilled Co$_4$Sb$_{12}$ prepared under high-pressure. Long Sb–Sb bonds display a similar distance in unfilled and filled samples, while the local thermal expansion coefficient in Gd-filled Co$_4$Sb$_{12}$ is much larger, suggesting a much weaker covalent interaction. This is in contrast with previously reported local thermal expansion coefficients of Yb$_{0.3}$Co$_4$Sb$_{12}$, in which the significant weakening of short Sb–Sb distances led towards more squared bond order of short and long Sb–Sb interactions. This lengthening is related to the change in electronic structure and population of antibonding states, leading to the band convergence, core of the excellent thermoelectric performance of filled Co$_4$Sb$_{12}$ [43]. In contrast, while Gd-filled Co$_4$Sb$_{12}$ still shows an increase of short Sb–Sb bond distances, the structure still retains a much stronger short Sb–Sb bond than long Sb–Sb bond, which is weakened. This is related to the low filling fraction and different electronic interactions of Gd^{3+} and Yb$^{3+/2+}$ within the skutterudite structure. Besides, as reported previously, Co–Sb bond nature remains unaltered after filling.

Table 2. Linear thermal expansion coefficients (α^L) evaluated for the bond Co–Sb, Sb–Sb, and M–Sb in both unfilled [19] and filled (M = Gd and Yb [41]) Co$_4$Sb$_{12}$ skutterudites, being normalized with respect to the 300 K bond length.

Preprints (www.preprints.org) | NOT PEER-REVIEWED | Posted: 21 November 2022 doi:10.20944/preprints202211.0389.v1

Structural parameter	α^L (×10^{-6} K^{-1})		
	Co_4Sb_{12}	$Gd_{0.066(4)}Co_4Sb_{12}$	$Yb_{0.3}Co_4Sb_{12}$
d_0 (Co–Sb)	8.9	9.1	9.1
d_1 (Sb–Sb)	9.7	9.6	12.6
d_2 (Sb–Sb)	12.7	16.8	15.9
d_3 (M–Sb)	-	7.3	8.6

3.5. Thermoelectric performance

The three main thermoelectric transport properties of the unfilled Co_4Sb_{12} and the $Gd_{0.066(4)}Co_4Sb_{12}$ composition are displayed in **Fig. 5**. There is a significant reduction of the resistivity (**Fig. 5a**) with the addition of the filler element, even in these small quantities, dropping down to ~10^{-5} Ω.m throughout the entire measurement range. Moreover, these values are slightly better than those reported for both $Gd_{0.09}Co_4Sb_{12}$ and $Gd_{0.12}Co_4Sb_{12}$ prepared at 4 GPa, which are between 2×10^{-5} Ω.m and 4×10^{-5} Ω.m [26]. Regarding the Seebeck coefficient, it shows a significant reduction at room temperature compared to -350 μV/K of the unfilled Co_4Sb_{12}, down to -100 μV/K for the Gd-filled compound (**Fig. 5b**). Such a drastic change in the Seebeck coefficient cannot only be attributed to the charge transfer from the filler element to the skutterudite framework, because the refined filling fraction is only x = 0.066(4). Instead, the change in this transport parameter is affected by both, the charge transfer and the change in the band structure induced by the filler element, the Gd atom. The lower Seebeck coefficient shown by this composition compared to that reported for the $Gd_xCo_4Sb_{12}$ specimen prepared at 4 GPa [26] (-260 μV/K at room temperature), together with the reduction in the resistivity, suggest that the charge transfer is more prominent in this sample. Nevertheless, this is inconsistent with lower filling fraction values and will be discussed below. The calculated power factor can be seen in **Fig. 5c**, exhibiting higher values than that of the undoped compound, but lower than those reported for other Gd-filled compounds [26].

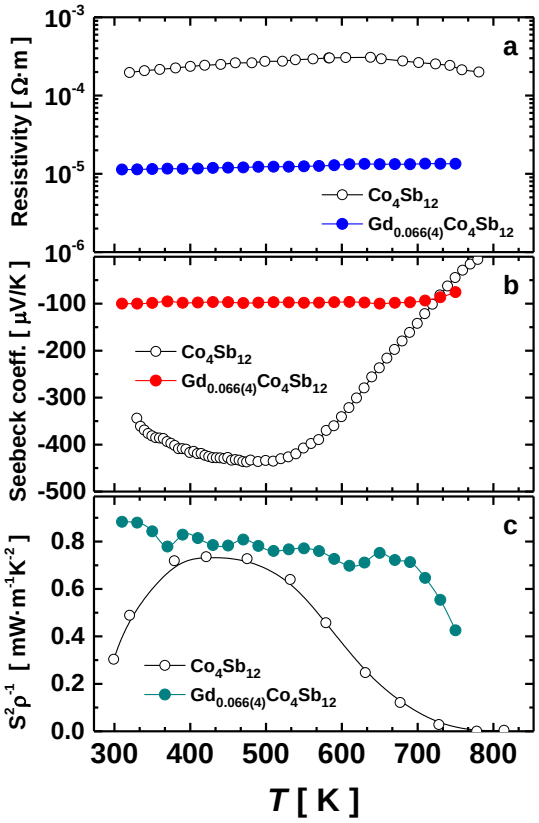

Figure 5. Temperature dependence of the: **(a)** resistivity, **(b)** Seebeck coefficient, and **(c)** power factor ($S^2\rho^{-1}$) of the Gd-filled skutterudite obtained under high-pressure conditions at 3.5 GPa.

Preprints (www.preprints.org) | NOT PEER-REVIEWED | Posted: 21 November 2022 doi:10.20944/preprints202211.0389.v1

The weighted mobility [44] of the Gd-filled compound calculated from the experimental Seebeck coefficient and resistivity is shown in **Fig. 6**. This mobility gives nearly the same information about carrier mobility as the Hall mobility, so we can extract some useful hints about the behavior of the charge carriers from the analysis of this plot. The main insight is that the electronic transport in this compound is limited by acoustic phonon scattering, an effect that can be noted by the decrease of the weighted mobility with temperature following a $T^{-3/2}$ relation. The weighted mobility of this Gd-filled derivative is comparatively higher than that of other filled skutterudites prepared by the same method [45]. Taking this into account, our samples may present a lower carrier concentration than expected, while the Seebeck coefficient is not as enhanced by band convergence as in other higher filling-fraction Gd-Co_4Sb_{12}. This agrees with the relationship of the filling fraction and doping level of antibonding states with conduction bands convergence, due to the low filling fraction values extracted from SXRD. Indeed, the structural analysis points towards the same argument, as the short Sb–Sb bonds still display lower values of thermal expansion and a much stronger interaction than that of long Sb–Sb bonds, while the opposite behavior would promote the band convergence [41].

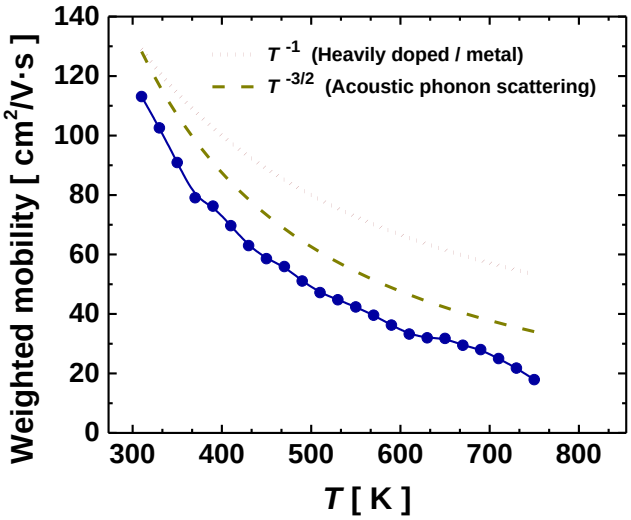

Figure 6. Calculated weighted mobility of the Gd-filled skutterudite obtained under high-pressure conditions at 3.5 GPa (dark blue symbols). The dotted and dashed lines exhibit the trends associated with different behaviors.

The total thermal conductivity is displayed in **Fig. 7a**. There is a huge reduction in the thermal conductivity of the Gd-filled composition compared to the unfilled one, as reported before for other filler elements [20–22]. The thermal conductivity becomes as low as 0.89 W/m.K at 773 K, lower than the minimum of ~3 W/m.K reported for other Gd-filled skutterudites synthesized at high-pressure [26], and the ~1.5–2 W/m.K reported for other doped skutterudites [46,47]. Such a decrease in the thermal conductivity is a consequence of the rattling behavior of the Gd atom which, as we described before, shows an intrinsic disorder parameter ~5× and ~25× higher than those of the Co and Sb atoms, respectively. Lastly, the calculated thermoelectric figure of merit (zT) is plotted in **Fig. 7b**. A maximum value of ~0.5 is achieved at 673 K, being approximately equal to that reported for both $Gd_{0.09}Co_4Sb_{12}$ and $Gd_{0.12}Co_4Sb_{12}$ compounds [26], but shifted towards higher temperatures.

Preprints (www.preprints.org) | NOT PEER-REVIEWED | Posted: 21 November 2022 doi:10.20944/preprints202211.0389.v1

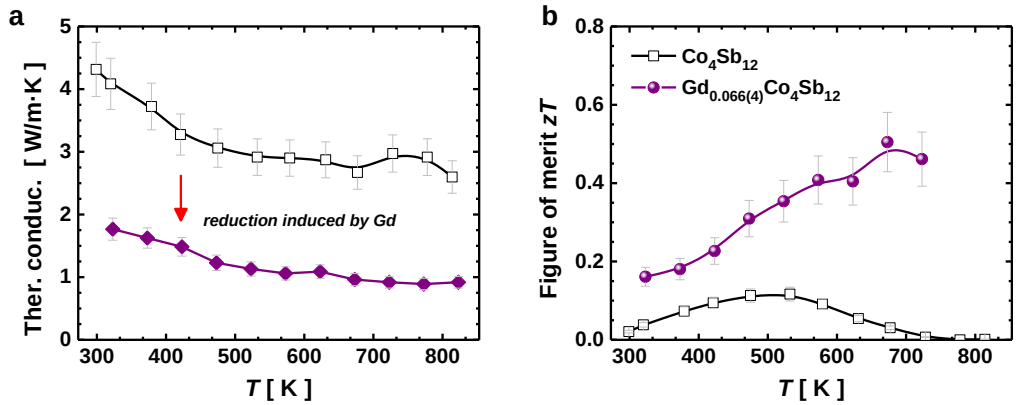

Figure 7. (a) Total thermal conductivity and **(b)** thermoelectric figure of merit (zT) of the unfilled and the Gd-filled compound obtained under high-pressure conditions at 3.5 GPa.

4. Conclusions

In short, Gd-filled skutterudite $Gd_xCo_4Sb_{12}$ was successfully synthesized in one-step method under high-pressure in a piston-cylinder press at 3.5 GPa and moderate temperature of 800 °C. Structural characterizations were performed using SXRD, from which a filling fraction of x = 0.066(4) and an average <Gd–Sb> bond length of 3.3499(3) Å were estimated. The lattice thermal expansion and lattice anharmonicity were studied via temperature-dependent SXRD. A Debye temperature of 322(3) K, from the fitting of the unit-cell volume expansion using the second order Grüneisen, was derived with a Grüneisen parameter γ' = 1.67(5). The Debye temperature was additionally evaluated from the mean square displacements of Co and Sb, leading to a value of 265(2) K. This difference means that the application of the harmonic Debye theory underestimates the Debye temperature in skutterudites. At the Gd sites, its intrinsic disorder value is ~5× and ~25× higher than those of Co and Sb, respectively, denoting that Gd has a strong rattling with an Einstein temperature of θ_E = 67(2) K. This rattling behavior promotes an ultra-low thermal conductivity of ~0.89 W/m·K at 773 K, explained from acoustic phonon scattering, which consequently leads to a thermoelectric efficiency zT of ~0.5 at 673 K.

Author Contributions: Conceptualization, J.E.R. and J.A.A.; methodology, J.E.R., J. G., F.S-S., R.S.S., C. D., N.M.N., O.J.D., J.L.M., and J.A.A.; formal analysis, J.E.R., J.A.A., and J.G.; resources, C. D., J.L.M. and J.A.A.; writing—original draft preparation, J.E.R., J.A.A., J.G., and F.S-S.; funding acquisition, J.L.M. and J.A.A. All authors have read and agreed to the published version of the manuscript.

Funding: We thank the Spanish Ministry of Science and Innovation for granting the project numbers: PID2021-122477OB-I00, TED2021-129254B-C22 and PRE2018-083398, funded by MCIN/AEI/10.13039/501100011033 and by "ERDF A way of making Europe", by the "European Union". Grants PIE: 2021-60-E-030 and PIE: 2010-6-OE-013 are also acknowledged.

Acknowledgments: All the authors acknowledge the European Synchrotron (ESRF, Grenoble) for making all the facilities available for the synchrotron X-ray diffraction measurements (proposal HC-4990). JG thanks MICINN for granting the contract PRE2018-083398.

Data availability: The datasets used and/or analyzed are available from the corresponding author on reasonable request.

Conflicts of Interest: The authors declare no conflict of interest.

Institutional Review Board Statement: Not applicable.

Informed Consent Statement: Not applicable.

References

1. Bell, L.E. Cooling, Heating, Generating Power, and Recovering Waste Heat with Thermoelectric Systems. *Science (80-.).* **2008**, *321*, 1457–1461, doi:10.1126/science.1158899.

2. Champier, D. Thermoelectric Generators: A Review of Applications. *Energy Convers. Manag.* **2017**, *140*, 167–181, doi:10.1016/j.enconman.2017.02.070.

3. Siddique, A.R.M.; Rabari, R.; Mahmud, S.; Heyst, B. Van Thermal Energy Harvesting from the Human Body Using Flexible Thermoelectric Generator (FTEG) Fabricated by a Dispenser Printing Technique. *Energy* **2016**, *115*, 1081–1091, doi:10.1016/j.energy.2016.09.087.

4. He, W.; Zhang, G.; Zhang, X.; Ji, J.; Li, G.; Zhao, X. Recent Development and Application of Thermoelectric Generator and Cooler. *Appl. Energy* **2015**, *143*, 1–25, doi:10.1016/j.apenergy.2014.12.075.

5. Yang, J.; Caillat, T. Thermoelectric Materials for Space and Automotive Power Generation. *MRS Bull.* **2006**, *31*, 224–229, doi:10.1557/mrs2006.49.

6. Snyder, G.J.; Toberer, E.S. Complex Thermoelectric Materials. *Nat. Mater.* **2008**, *7*, 105–114, doi:10.1038/nmat2090.

7. Sales, B.C.; Mandrus, D.; Williams, R.K. Filled Skutterudite Antimonides: A New Class of Thermoelectric Materials. *Science (80-.).* **1996**, *272*, 1325–1328, doi:10.1126/science.272.5266.1325.

8. Liu, Z.-Y.; Zhu, J.-L.; Tong, X.; Niu, S.; Zhao, W.-Y. A Review of CoSb3-Based Skutterudite Thermoelectric Materials. *J. Adv. Ceram.* **2020**, *9*, doi:10.1007/s40145-020-0407-4.

9. Liu, W.S.; Zhang, B.P.; Li, J.F.; Zhang, H.L.; Zhao, L.D. Enhanced Thermoelectric Properties in CoSb3-x Tex Alloys Prepared by Mechanical Alloying and Spark Plasma Sintering. *J. Appl. Phys.* **2007**, *102*, doi:10.1063/1.2815671.

10. Sergueev, I.; Glazyrin, K.; Kantor, I.; McGuire, M.A.; Chumakov, A.I.; Klobes, B.; Sales, B.C.; Hermann, R.P. Quenching Rattling Modes in Skutterudites with Pressure. *Phys. Rev. B* **2015**, *91*, 224304, doi:10.1103/PhysRevB.91.224304.

11. Nolas, G.S.; Kendziora, C.A. Raman Spectroscopy Investigation of Lanthanide-Filled and Unfilled Skutterudites. *Phys. Rev. B - Condens. Matter Mater. Phys.* **1999**, *59*, 6189–6192, doi:10.1103/PhysRevB.59.6189.

12. Nolas, G.S.; Sharp, J.; Goldsmid, H.J. The Phonon—Glass Electron-Crystal Approach to Thermoelectric Materials Research. In; 2001; pp. 177–207.

13. Nolas, G.S.; Takizawa, H.; Endo, T.; Sellinschegg, H.; Johnson, D.C. Thermoelectric Properties of Sn-Filled Skutterudites. *Appl. Phys. Lett.* **2000**, *77*, 52–54, doi:10.1063/1.126874.

14. Sales, B.C.; Chakoumakos, B.C.; Mandrus, D. Thermoelectric Properties of Thallium-Filled Skutterudites. *Phys. Rev. B* **2000**, *61*, 2475–2481, doi:10.1103/PhysRevB.61.2475.

15. Pei, Y.Z.; Chen, L.D.; Zhang, W.; Shi, X.; Bai, S.Q.; Zhao, X.Y.; Mei, Z.G.; Li, X.Y. Synthesis and Thermoelectric Properties of KyCo 4Sb12. *Appl. Phys. Lett.* **2006**, *89*, 16–19, doi:10.1063/1.2397538.

16. Zhao, X.Y.; Shi, X.; Chen, L.D.; Zhang, W.Q.; Zhang, W.B.; Pei, Y.Z. Synthesis and Thermoelectric Properties of Sr-Filled Skutterudite SryCo4Sb12. *J. Appl. Phys.* **2006**, *99*, 053711, doi:10.1063/1.2172705.

17. Patschke, R.; Zhang, X.; Singh, D.; Schindler, J.; Kannewurf, C.R.; Lowhorn, N.; Tritt, T.; Nolas, G.S.; Kanatzidis, M.G. Thermoelectric Properties and Electronic Structure of the Cage Compounds A2BaCu8Te10 (A = K, Rb, Cs): Systems with Low Thermal Conductivity. *Chem. Mater.* **2001**, *13*, 613–621, doi:10.1021/cm000390o.

18. Snyder, G.J.; Christensen, M.; Nishibori, E.; Caillat, T.; Iversen, B.B. Disordered Zinc in Zn4Sb3 with Phonon-Glass and Electron-Crystal Thermoelectric Properties. *Nat. Mater.* **2004**, *3*, 458–463, doi:10.1038/nmat1154.

19. Prado-Gonjal, J.; Serrano-Sánchez, F.; Nemes, N.M.; Dura, O.J.; Martínez, J.L.; Fernández-Díaz, M.T.; Fauth, F.; Alonso, J.A. Extra-Low Thermal Conductivity in Unfilled CoSb3-δ Skutterudite Synthesized under High-Pressure Conditions. *Appl. Phys. Lett.* **2017**, *111*, 1–6, doi:10.1063/1.4993283.

20. Serrano-Sánchez, F.; Prado-Gonjal, J.; Nemes, N.M.; Biskup, N.; Varela, M.; Dura, O.J.; Martínez, J.L.; Fernández-Díaz, M.T.; Fauth, F.; Alonso, J.A. Low Thermal Conductivity in La-Filled Cobalt Antimonide Skutterudites with an Inhomogeneous Filling Factor Prepared under High-Pressure Conditions. *J. Mater. Chem. A* **2017**, *6*, 118–126, doi:10.1039/c7ta08545a.

21. Gainza, J.; Serrano-Sánchez, F.; Prado-Gonjal, J.; Nemes, N.M.; Biskup, N.; Dura, O.J.; Martínez, J.L.; Fauth, F.; Alonso, J.A. Substantial Thermal Conductivity Reduction in Mischmetal Skutterudites Mm x Co 4 Sb 12 Prepared under High-Pressure Conditions, Due to Uneven Distribution of the Rare-Earth Elements. *J. Mater. Chem. C* **2019**, *7*, 4124–4131, doi:10.1039/C8TC06461J.

22. Serrano-Sánchez, F.; Prado-Gonjal, J.; Nemes, N.M.; Biskup, N.; Dura, O.J.; Martínez, J.L.; Fernández-Díaz, M.T.; Fauth, F.; Alonso, J.A. Thermal Conductivity Reduction by Fluctuation of the Filling Fraction in Filled Cobalt Antimonide Skutterudite Thermoelectrics. *ACS Appl. Energy Mater.* **2018**, *1*, 6181–6189, doi:10.1021/acsaem.8b01227.

23. Gainza, J.; Serrano-Sánchez, F.; Rodrigues, J.E.; Prado-Gonjal, J.; Nemes, N.M.; Biskup, N.; Dura, O.J.; Martínez, J.L.; Fauth, F.; Alonso, J.A. Unveiling the Correlation between the Crystalline Structure of M-Filled CoSb 3 (M = Y, K, Sr) Skutterudites and Their Thermoelectric Transport Properties. *Adv. Funct. Mater.* **2020**, *30*, 2001651, doi:10.1002/adfm.202001651.

24. Rodrigues, J.E.F.S.; Gainza, J.; Serrano-Sánchez, F.; Marini, C.; Huttel, Y.; Nemes, N.M.; Martínez, J.L.; Alonso, J.A. Atomic Structure and Lattice Dynamics of CoSb $_3$ Skutterudite-Based Thermoelectrics. *Chem. Mater.* **2022**, *34*, 1213–1224, doi:10.1021/acs.chemmater.1c03747.

25. Rodrigues, J.E.F.S.; Gainza, J.; Serrano-Sánchez, F.; Ferrer, M.M.; Fabris, G.S.L.; Sambrano, J.R.; Nemes, N.M.; Martínez, J.L.; Popescu, C.; Alonso, J.A. Unveiling the Structural Behavior under Pressure of Filled M 0.5 Co 4 Sb 12 (M = K, Sr, La, Ce, and Yb) Thermoelectric Skutterudites. *Inorg. Chem.* **2021**, *60*, 7413–7421, doi:10.1021/acs.inorgchem.1c00682.

26. Yang, J.; Xu, B.; Zhang, L.; Liu, Y.; Yu, D.; Liu, Z.; He, J.; Tian, Y. Gadolinium Filled CoSb3: High Pressure Synthesis and Thermoelectric Properties. *Mater. Lett.* **2013**, *98*, 171–173, doi:10.1016/j.matlet.2013.02.034.

27. Liu, R.; Chen, X.; Qiu, P.; Liu, J.; Yang, J.; Huang, X.; Chen, L. Low Thermal Conductivity and Enhanced Thermoelectric Performance of Gd-Filled Skutterudites. *J. Appl. Phys.* **2011**, *109*, 023719, doi:10.1063/1.3533743.

28. Fitch, A.; Dejoie, C. Combining a Multi-Analyzer Stage with a Two-Dimensional Detector for High-Resolution Powder X-Ray Diffraction: Correcting the Angular Scale. *J. Appl. Crystallogr.* **2021**, *54*, 1088–1099, doi:10.1107/S1600576721005288.

29. Rodríguez-Carvajal, J. Recent Advances in Magnetic Structure Determination by Neutron Powder Diffraction. *Phys. B Phys. Condens. Matter* **1993**, *192*, 55–69, doi:10.1016/0921-4526(93)90108-I.

30. Vočadlo, L.; Knight, K.S.; Price, G.D.; Wood, I.G. Thermal Expansion and Crystal Structure of FeSi between 4 and 1173 K Determined by Time-of-Flight Neutron Powder Diffraction. *Phys. Chem. Miner.* **2002**, *29*, 132–139, doi:10.1007/s002690100202.

31. Vočadlo, N.L.; Price, G.D. The Grüneisen Parameter — Computer Calculations via Lattice Dynamics. *Phys. Earth Planet. Inter.* **1994**, *82*, 261–270, doi:10.1016/0031-9201(94)90076-0.

32. Shirotani, I.; Noro, T.; Hayashi, J.; Sekine, C.; Giri, R.; Kikegawa, T. X-Ray Study with Synchrotron Radiation for P- and Sb-Based Skutterudite Compounds at High Pressures. *J. Phys. Condens. Matter* **2004**, *16*, 7853–7862, doi:10.1088/0953-8984/16/43/024.

33. Nielsen, M.D.; Ozolins, V.; Heremans, J.P. Lone Pair Electrons Minimize Lattice Thermal Conductivity. *Energy Environ. Sci.* **2013**, *6*, 570–578, doi:10.1039/C2EE23391F.

34. Abia, C.; López, C.A.; Gainza, J.; Rodrigues, J.E.F.S.; Ferrer, M.M.; Nemes, N.M.; Dura, O.J.; Martínez, J.L.; Fernández-Díaz, M.T.; Álvarez-Galván, C.; et al. The Structural Evolution, Optical Gap, and Thermoelectric Properties of the RbPb2Br5 Layered Halide, Prepared by Mechanochemistry. *J. Mater. Chem. C* **2022**, *10*, 6857–6865, doi:10.1039/D2TC00653G.

35. Nakatsuka, A.; Yoshiasa, A.; Fujiwara, K.; Ohtaka, O. Variable-Temperature Single-Crystal X-Ray Diffraction Study of SrGeO3 High-Pressure Perovskite Phase. *J. Mineral. Petrol. Sci.* **2018**, *113*, 280–285, doi:10.2465/jmps.180605.

36. Rodrigues, J.E.F.S.; Escanhoela, C.A.; Fragoso, B.; Sombrio, G.; Ferrer, M.M.; Álvarez-Galván, C.; Fernández-Díaz, M.T.; Souza, J.A.; Ferreira, F.F.; Pecharromán, C.; et al. Experimental and Theoretical Investigations on the Structural, Electronic, and Vibrational Properties of Cs 2 AgSbCl 6 Double Perovskite. *Ind. Eng. Chem. Res.* **2021**, acs.iecr.1c02188, doi:10.1021/acs.iecr.1c02188.

37. Mi, J.-L.; Christensen, M.; Nishibori, E.; Iversen, B.B. Multitemperature Crystal Structures and Physical Properties of the Partially Filled Thermoelectric Skutterudites M0.1Co4Sb12 (M = La,Ce,Nd,Sm,Yb and Eu). *Phys. Rev. B* **2011**, *84*, 064114, doi:10.1103/PhysRevB.84.064114.

38. de Abrantes, J.G.; Cantarino, M.R.; da Silva Neto, W.R.; Freire, V. V.; Figueiredo, A.G.; Germano, T.M.; Mounssef, B.; Bittar, E.M.; Leithe-Jasper, A.; Garcia, F.A. Vibrational and Structural Properties of the RFe4Sb12 (R = Na, K, Ca, Sr, Ba) Filled Skutterudites. *Phys. Rev. Mater.* **2022**, *6*, 085403, doi:10.1103/PhysRevMaterials.6.085403.

39. Morelli, D.T.; Meisner, G.P. Low Temperature Properties of the Filled Skutterudite CeFe 4 Sb 12. *J. Appl. Phys.* **1995**, *77*, 3777–3781, doi:10.1063/1.358552.

40. Uher, C. Chapter 5 Skutterudites: Prospective Novel Thermoelectrics. In *Semiconductors and Semimetals*; 2001; Vol. 69, pp. 139–253 ISBN 012752178X.

41. Hanus, R.; Guo, X.; Tang, Y.; Li, G.; Snyder, G.J.; Zeier, W.G. A Chemical Understanding of the Band Convergence in Thermoelectric CoSb3 Skutterudites: Influence of Electron Population, Local Thermal Expansion, and Bonding Interactions. *Chem. Mater.* **2017**, *29*, 1156–1164, doi:10.1021/acs.chemmater.6b04506.

42. Oftedal, I. The Crystal Structure of Skutterudite and Related Minerals. *Nor. Geol. Tidsskr.* **1926**, *8*, 250–257.

43. Tang, Y.; Gibbs, Z.M.; Agapito, L.A.; Li, G.; Kim, H.S.; Nardelli, M.B.; Curtarolo, S.; Snyder, G.J. Convergence of Multi-Valley Bands as the Electronic Origin of High Thermoelectric Performance in CoSb3 Skutterudites. *Nat. Mater.* **2015**, *14*, 1223–1228, doi:10.1038/nmat4430.

44. Snyder, G.J.; Snyder, A.H.; Wood, M.; Gurunathan, R.; Snyder, B.H.; Niu, C. Weighted Mobility. *Adv. Mater.* **2020**, *32*, 2001537, doi:10.1002/adma.202001537.

45. Gainza, J.; Serrano-Sánchez, F.; Nemes, N.M.; Dura, O.J.; Martínez, J.L.; Fauth, F.; Alonso, J.A. Strongly Reduced Lattice Thermal Conductivity in Sn-Doped Rare-Earth (M) Filled Skutterudites M x Co 4 Sb 12−y Sn y , Promoted by Sb–Sn Disordering and Phase Segregation. *RSC Adv.* **2021**, *11*, 26421–26431, doi:10.1039/D1RA04270J.

46. Meledath Valiyaveettil, S.; Nguyen, D.L.; Wong, D.P.; Hsing, C.R.; Paradis-Fortin, L.; Qorbani, M.; Sabbah, A.; Chou, T.L.; Wu, K.K.; Rathinam, V.; et al. Enhanced Thermoelectric Performance in Ternary Skutterudite Co(Ge0.5Te0.5)3via Band Engineering. *Inorg. Chem.* **2022**, *61*, 4442–4452, doi:10.1021/acs.inorgchem.1c03947.

47. Meledath Valiyaveettil, S.; Qorbani, M.; Hsing, C.-R.; Chou, T.-L.; Paradis-Fortin, L.; Sabbah, A.; Srivastava, D.; Nguyen, D.-L.; Ho, T.-T.; Billo, T.; et al. Enhanced Thermoelectric Performance of Skutterudite Co1−yNiySn1.5Te1.5−x with Switchable Conduction Behavior. *Mater. Today Phys.* **2022**, *28*, 100889, doi:10.1016/j.mtphys.2022.100889.